HHS Public Access

Author manuscript

Curr Biol. Author manuscript; available in PMC 2022 August 23.

Published in final edited form as:

Curr Biol. 2021 August 23; 31(16): 3639–3647.e5. doi:10.1016/j.cub.2021.05.061.

Capicua is a fast-acting transcriptional brake

Aleena L. Patel[1,2,3], **Lili Zhang**[5], **Shannon E. Keenan**[1,2,3], **Christine A. Rushlow**[4], **Cécile Fradin**[5,7,*], **Stanislav Y. Shvartsman**[2,3,6,8,*]

[1]Department of Chemical and Biological Engineering, Princeton University, Princeton, NJ 08540, USA

[2]Department of Molecular Biology, Princeton University, Princeton, NJ 08540, USA

[3]Lewis-Sigler Institute for Integrative Genomics, Princeton University, Princeton, NJ 08540, USA

[4]Department of Biology, New York University, New York, NY 10003, USA

[5]Department of Physics and Astronomy, McMaster University, Hamilton, ON L8S 4K1, Canada

[6]Center for Computational Biology, Flatiron Institute, New York, NY 10010, USA

[7]Department of Biochemistry and Biomedical Sciences, McMaster University, Hamilton, ON L8S 4K1, Canada

[8]Lead contact

SUMMARY

Even though transcriptional repressors are studied with ever-increasing molecular resolution, the temporal aspects of gene repression remain poorly understood. Here, we address the dynamics of transcriptional repression by Capicua (Cic), which is essential for normal development and is commonly mutated in human cancers and neurodegenerative diseases.[1,2] We report the speed limit for Cic-dependent gene repression based on live imaging and optogenetic perturbations in the early *Drosophila* embryo, where Cic was originally discovered.[3] Our measurements of Cic concentration and intranuclear mobility, along with real-time monitoring of the activity of Cic target genes, reveal remarkably fast transcriptional repression within minutes of removing an optogenetic de-repressive signal. In parallel, quantitative analyses of transcriptional bursting of Cic target genes support a repression mechanism providing a fast-acting brake on burst generation. This work sets quantitative constraints on potential mechanisms for gene regulation by Cic.

In brief

Patel et al. report the timescale of transcriptional repression by Capicua in the early *Drosophila* embryo. Biophysical properties of Capicua are measured in interphase nuclei. Optimized

*Correspondence: fradin@physics.mcmaster.ca (C.F.), stas@princeton.edu (S.Y.S.).

AUTHOR CONTRIBUTIONS

A.L.P., C.F., and S.Y.S. generated the ideas and designed the experiments with input from C.A.R. A.L.P. and L.Z. performed the experiments. S.E.K. generated the *hkb* MS2 reporter line. A.L.P. wrote the paper with input from C.A.R., C.F., and S.Y.S.

SUPPLEMENTAL INFORMATION

Supplemental information can be found online at https://doi.org/10.1016/j.cub.2021.05.061.

DECLARATION OF INTERESTS

The authors declare no competing interests.

photoswitchable MEK toggles gene repression. Optogenetic perturbations and live reporters of nascent transcript production reveal fast-acting gene repression.

RESULTS AND DISCUSSION

Transcriptional repressors provide molecular brakes on gene expression circuits at key moments in time and in precise spatial patterns during embryogenesis and homeostasis.[4-6] The high-mobility group (HMG)-box transcription factor and repressor Capicua (Cic) regulates cell fate decisions during development and acts as a tumor suppressor in adult tissues.[2,7,8] From fruit flies to humans, Cic mediates inductive receptor tyrosine kinase (RTK) signaling.[1,9-11] In the absence of RTK signals, Cic represses target genes, many of which are known oncogenes involved in cell proliferation.[12] Exposing cells to ligands that bind RTKs activates the extracellular signal-regulated kinase (ERK) cascade, which counteracts Cic repression, analogous to releasing the brake pedal of a car, to induce target gene transcription.[5,13]

The current quantitative models for Cic-dependent gene control rely on studies of the initial pulse of RTK activation in the *Drosophila* blastoderm, during 13 synchronous nuclear divisions spanning the first 2 h post-fertilization (hpf).[5,14] In this time window, Cic regulates expression of *tailless* (*tll*) and *huckebein* (*hkb*), genes required for distinguishing the head and tail from mid-body segmented structures of the emerging larva (Figure 1A).[15-17] A bipartite structure formed between the HMG-box and a C1 domain allows Cic to specifically recognize the conserved octameric DNA binding site “TGAATGAA” in the regulatory elements of *tll* and *hkb*.[9,18] Activation of ERK by locally produced ligands at the anterior and posterior poles phosphorylates Cic to relieve repression, causing Cic unbinding from DNA and export from the nucleus for eventual degradation.[19,20] Consequently, Cic de-repression is described as a two-step process: fast relief of repression upon Cic phosphorylation and unbinding from DNA, followed by slower changes in Cic subcellular localization and stability.

We currently lack such a detailed and quantitative understanding of the molecular mechanisms for establishing repression by Cic. It is particularly important to address this question in contexts where Cic levels are depleted by active and sustained ERK signaling. Signal-dependent control of Cic concentration might be a physiologically important mechanism for long-term memory of ERK activation; the slower steps of Cic de-repression may deplete enough repressor to sustain transcription after ERK signals are removed, a hypothesis that we are interested in testing. We manipulated Cic function with spatially uniform optogenetic signal perturbations in nuclei found in the middle of the *Drosophila* embryo after the 13th mitotic division (interphase of nuclear cycle “nc” 14). Prior studies of short (5-min) pulsed optogenetic signals suggest that this tissue has the potential to reveal the fastest timescales of transcriptional control, but these perturbations were insufficient to access the timescale of establishing a repressed state from scratch.[20] Here, we directly determine the speed limit of *de novo* Cic-responsive gene repression with hours-long sustained and step-like perturbations using a photoswitchable form of ERK’s kinase, MEK.[21]

The optogenetic tool we used, optimized photoswitchable MEK (psMEK), activates ERK to at least the endogenous active ERK levels at the poles, which have been shown to reduce nuclear Cic concentration about 10-fold (Figure 1B).[19,22] Knowing this, we measured Cic diffusivity and concentration in nuclei free of endogenous ERK signals in the middle of embryos to quantitatively gauge how rate limiting the mobility parameters might be during the early stages of embryogenesis. Cic endogenously tagged with superfolder GFP (sfGFP) was imaged via confocal microscopy (Figure 1C). Fluorescence recovery after photobleaching (FRAP) established that Cic-sfGFP molecules became uniformly distributed less than 3 s after photobleaching a portion of the nucleus, suggesting that there is no significant immobile fraction on the ~1-s timescale (Figure 1D). Fluorescence correlation spectroscopy (FCS) revealed two populations of Cic molecules: a fast-diffusing fraction with a residence time in the confocal detection volume of less than 1 ms (median diffusion coefficient 32 $\mu m^2/s$) and a slower moving population with a residence time of about 60 ms (Figure 1E). The slower population could consist of molecules that are transiently part of larger molecular complexes or phase-separated repressive droplets (moving with an apparent diffusion coefficient of 0.4 $\mu m^2/s$). It could also indicate transient DNA binding on the 60-ms timescale, which would be relevant for transcriptional repression.[23] No matter what the interpretation for this slowing down of a fraction of the Cic population is, the effective mobility of Cic (taking into account both the fast and slow population) can be given as D_{eff} = 20 $\mu m^2/s$ (median value for all measurements in nc 13 and 14).

Cic is not only quickly diffusing but also abundant compared to the number of binding loci in the genome. Concentration could be measured from the FCS experiments (Figure S1). In nc 14, the measured concentration was ~240 nM (Figure 1F). Because each nc 14 nucleus has a radius of ~3 μm, there are ~20,000 Cic molecules per nucleus, which is roughly two orders of magnitude larger than the number of Cic-binding loci in the *Drosophila* genome identified by chromatin immunoprecipitation sequencing (ChIP-seq) (Figure 1G).[20] Optogenetically ERK-activated nuclei would have around 2,000 molecules, putting Cic concentration in a range that may allow for sensitive and rapid switching of the transcriptional state.[19,24]

Our measurements of Cic diffusivity and concentration provide an estimate of the time for Cic to search for its binding site in the nucleus via the Smoluchowski equation (Figure 1G).[25] As a demonstration, we considered the target length “a” to be 7.7 nm (the sum of the size of a protein and an octameric binding site) and plotted the resulting search times using a range of plausible values for D_{eff} (12–29 $\mu m^2/s$) and C (225–262 nM), given the dispersion in our measurements (Figure 1H). The range of search times was ~3–6 ms and remains in the sub-second timescale, even when the length constraint is relaxed (3 ms for D = 23 $\mu m^2/s$, a = 5 nm, and C = 290 nM and 150 ms for D = 12 $\mu m^2/s$, a = 0.34 nm, and C = 130 nM). Reducing Cic levels by an order of magnitude with optogenetic ERK signals would still result in a search time on the sub-second timescale. These estimates provide a hypothesis that Cic represses transcription quickly if a strong optogenetic ERK signal is removed. However, mobility measurements of Cic do not address other features of transcription factor searching, such as local access to binding sites regulated by chromatin architecture or interactions with additional regulators like the co-repressor Groucho.[3,26]

Thus, the biologically relevant response, transcription of Cic-responsive target genes, must be measured.

Here, we used the MS2-MCP (MS2 coat protein) system in *Drosophila* to report nascent mRNA production while optogenetically toggling ERK activation in nc 14 with optimized psMEK (Figure 2A).[27] As MS2 stem loops genetically engineered into the reporters are transcribed, MCP fluorescently tagged with mCherry binds to the loops. Concentrated mCherry is visible via confocal microscopy as a bright spot in nuclei. The optimized psMEK tool conveniently circumvents potential delays in signal transduction via upstream components of the pathway, as it directly phosphorylates ERK, and acts only one node away from Cic in the signal transduction cascade. 500 nm light activates optimized psMEK by dissociating domains that sterically hinder MEK's active site. 400 nm light inactivates it by closing the domains over the active site.[21,22,28]

psMEK perturbations confirm that transcription repression is established very quickly, even after sustained illumination and ERK activation from the time of egg lay (spanning ~2 h). We combined the tool with an MS2 reporter for *tll* that contains fragments of the regulatory DNA (*tll**) used in previous studies.[20] Embryos were illuminated with psMEK-activating light from egg laying to nc 14. MS2 transcriptional activity was sustained with continued illumination for 2 min after the completion of the nc 13 to nc 14 mitosis. Signaling was then abruptly terminated by switching illumination to the psMEK-inactivating wavelength. *tll** transcription, quantified as the percent of the nuclei in the field of view with an MS2-MCP spot per time frame, declined rapidly upon inactivating optimized psMEK (Figure 2B). Transcriptional repression by Cic occurs within minutes of removing the sustained ERK signal (Figure 2C).

The MS2-MCP imaging reveals a highly regulated sequence of events, called "bursting," which reflects periods of active mRNA generation followed by transcriptional quiescence.[29,30] Fluctuating signals were characterized for transcriptional states established with two optogenetic perturbations: continuous and photoswitched MEK activation in nuclei from the middle of embryos in nc 14. MS2 loops inserted via CRISPR near the *hkb* gene body reported endogenous activity of an ERK target gene other than *tll* (Figure 3A). We illuminated embryos with psMEK-activating light from the time of egg lay to fully derepress transcription. For each time point, multiple bright foci of mCherry fluorescence, indicating MCP binding to MS2 loops, were detected. The maximum recorded spot intensity was plotted over time to display how transcriptional activity appeared throughout nc 14 (Figure 3Bi). Individually tracked spots revealed discontinuous transcription with several intensity peaks throughout nc 14, which collectively contributed to signal detection for at least 15 min (Figure 3Bii). In other embryos, we switched illumination to the psMEK-inactivating wavelength immediately after the nc 13 to nc 14 mitosis, thereby allowing Cic to repress transcription. In the movies of embryos subject to repression by Cic, because of the rapidly removed optogenetic ERK signal, the maximum spot intensity dropped dramatically after 5 min (Figure 3Ci). Individually tracked spots in this short time window of repression appeared to reach only one peak, indicative of single bursts (Figure 3Cii). Thus, Cic is a fast-acting brake on endogenous gene transcription that appears to limit bursting to an ~5-min time window.

To test whether the fast-acting brake is dependent on the presence of Cic binding sites, we performed similar perturbations and spot quantifications in embryos expressing a newly constructed RTK-sensitive reporter. We introduced 4 Cic binding sites (TGAATGAA) near the regulatory region of *bottleneck* (*bnk*), which does not contain Cic sites, driving MS2 loops (Figure 3D). In embryos expressing this reporter, MS2 activity was only apparent at the poles, reflecting endogenous ERK signals (Figure S2A). A similar reporter constructed with only one intact Cic site and three mutated Cic sites expressed uniformly (Figure S2B), suggesting that the 4 Cic binding sites were important for the observed restricted expression at the poles.

Activating optimized psMEK to continually lift the repressive Cic brake on transcription in embryos with the *bnk* + 4 Cic sites reporter led to sustained transcription in the middle of the embryo throughout nc 14 (Figure 3E). The apparent decline in maximum spot intensity could reflect a direct readout of falling levels of the transcriptional activator, Zelda, known to regulate *bnk*, as the embryo undergoes the maternal to zygotic transition (MZT).[31] A control reporter with no intact Cic sites added upstream of the *bnk* enhancer also showed a decline in transcription (Figure S3). Even for such a reporter that may be very sensitive to dynamics of the activator, removing the optogenetic ERK signal reapplied the Cic transcriptional brake quickly (Figure 3F).

We then compared quantitative features of the apparent bursts of transcription subjected to repression by Cic in nc 14 with bursts subjected to continued ERK activation (de-repressed transcription). Tracked fluorescent spots were extracted from the first 6 min of nc 14, to fairly compare the two conditions (Figure 4A). Here, spot tracking did not allow for periods of transcriptional quiescence, so sequential “bursts” in the same nucleus were recorded as multiple individually tracked spots. The lifetimes and maximum intensities (peaks) of spots from movies of embryos treated under the same optogenetic conditions (repressed or de-repressed transcription) were pooled to generate distributions for each parameter. For *hkb*, the spot lifetimes, corresponding to the apparent burst durations, of repressed and de-repressed bursts were found to belong to the same distribution by a Kolmogorov-Smirnov test. Spot peak intensity distributions were significantly different, but repression did not drastically dim bursts (Figure 4B).

Similar spot measurements performed for the modified *bnk* + 4 Cic sites reporter, which uses a different MS2 stem loop sequence, also suggest that Cic repression does not drastically alter individual bursts (Figure 4C).[32] To further ensure that our measurements were from a reporter that is sensitive enough to our optogenetic perturbation, we compared apparent bursts from the continually de-repressed nuclei to apparent bursts from the *bnk* reporter with no intact Cic binding sites (Figure S4). De-repressed bursts from the *bnk* + 4 Cic sites reporter were similar to bursts from the non Cic-dependent *bnk* reporter, indicating that the ERK signals are revealing the expected transcriptional activity. In sum, repression by Cic does not appear to change the nature of individual transcriptional bursts.

Bursts may remain unchanged upon repression by Cic if an immediate removal of the de-repressive ectopic ERK signal, or “hard brake” enabled by photoswitching MEK, only interferes with transcription burst generation (Figure 4D). We define a potential hard brake

on transcription following the photoswitch of MEK and ERK as a mechanism that affects the onset of transcription but would not truncate nascent transcripts mid-elongation. This interpretation is consistent with previous work suggesting transcription initiation and RNA polymerase II (RNA Pol II) release are key points of gene control in this embryo and for mammalian genes.[33,34] If Cic primarily regulates burst generation, there could be a lag in gene silencing due to continued transcriptional elongation after the onset of repression. This scenario has been reported for the Zn-finger repressor Snail, where the time to complete transcriptional quiescence is a function of the size of the gene.[35] The burst initiation time at the start of nc 14 would be a lower bound on the time it takes for Cic to repress ERK target genes if Cic primarily acts to prevent a second burst (Figure 4E). This lower bound is slightly longer for the *bnk* + 4 Cic sites reporter, perhaps reflecting different dynamics of activator inputs to *bnk*.

These temporal bounds place quantitative limits on the molecular mechanisms of repression by Cic. Potential fast-acting mechanisms that would suppress burst generation include enhancer or promoter binding competition with activators or basal factors, disruption of the pre-initiation complex, altered interactions between RNA Pol II and elongation factors, or RNA Pol II pausing, implicated in repression by Cic's co-repressor Groucho.[31,36-40] The currently proposed mechanisms for gene repression by Cic in glioblastoma cells involve histone deacetylation.[41] It has not yet been shown that such epigenetic gene silencing mediates Cic repression in the early *Drosophila* embryo or whether histone deacetylation leads to rapid transcription shutdown. As an illustration, histone deacetylation occurs ~20 min after another mammalian repressor, Ikaros, binds to DNA. Interestingly, quicker changes to promoter accessibility, such as RNA polymerase eviction and altered nucleosome occupancy, silence Ikaros target gene transcription within 5–10 min, before histones are deacetylated.[42] The time window following the ERK photoswitch that we have captured encompasses the initial steps of Cic-mediated repression that rapidly deplete transcript, much like the immediate silencing of Ikaros targets. Here, we have not yet assayed potentially slower chromatin-level effects, such as how Cic-responsive gene loci might be repositioned into repressive micro-environments for more stable repression after loss of transcription.

Our work paints a picture of fast-acting mechanisms controlling nascent transcript generation in response to fluctuating signals in the early *Drosophila* embryo. Importantly, we also bring into question the function of two-step de-repression if Cic export and degradation do not limit the Cic binding search or transcriptional silencing rates. Quickly plunging a gene-regulatory system into a repressive state, as we have done using optogenetic manipulations of Cic, will be crucial for our emerging quantitative understanding of gene regulation relevant to both fundamental biology and disease.

STAR ★METHODS

RESOURCE AVAILABILITY

Lead contact—Further information and requests for resources should be directed to and will be fulfilled by the Lead Contact, Stas Shvartsman (stas@princeton.edu).

Materials availability—Fly lines generated in this study are listed in the Key resources table and are available at the laboratory upon request.

Data and code availability—Raw image data is available upon request.

EXPERIMENTAL MODEL AND SUBJECT DETAILS

Cic-sfGFP/+,[20] UAS-psMEKE203K[22] *tll*-MS2, MCP-mCherry (provided by the Levine lab), *hkb*-MS2 (this study), *bnk+4Cic*-MS2 (this study) and P(matα-GAL-VP16)mat67; P(matα-GAL-VP16)mat15 stocks[43] were used in this study. Cic-sfGFP represents Cic endogenously tagged with superfolder GFP.[46] Flies were kept at room temperature in vials containing a standard mixture of agar, cornmeal, and yeast, provided by the *Drosophila* Media Core Facility within the Princeton Molecular Biology Department. To collect embryos, flies were placed in cages with an agar plate made with apple juice and supplemented with a yeast paste.

METHOD DETAILS

FRAP—FRAP measurements were conducted for embryos endogenously expressing Cic-sfGFP. Embryos laid on agar plates were collected, dechorionated by hand, placed on their lateral side on a microscope coverslip covered with a very thin layer of heptane glue, then covered in halocarbon oil 700. Imaging and photobleaching were performed using a Nikon Eclipse Ti inverted confocal microscope. A rectangular region covering about half of a nucleus in the mid section of the embryo was photobleached at high laser power for 3 s, then the whole nucleus was immediately imaged at low laser power. As a control, the vitelline membrane of the embryo (which contains immobile fluorescence molecules) was also photobleached and imaged in the same conditions as the nucleus.

FCS—Embryos were collected and prepared as explained in the FRAP section. FCS measurements were performed using an Insight confocal instrument (Evotec Technologies, Hamburg). The radius of the detection volume, w_0, half-height Sw_0, and volume $V = \pi^{3/2} S w_0^3$, were obtained from measurements of the diffusion of a well characterized fluorophore (Alexa 488, diffusion coefficient $D = 435\ \mu m^2/s$).[47] All measurements were performed in the middle part of the embryo, only ~10 μm above the glass coverslip to avoid optical aberrations. In each studied nucleus, 10 successive FCS measurements (each lasting between 5 and 20 s) were performed in the middle of the nucleus. Noticeable photobleaching was systematically observed, even though a low 20 μW excitation intensity was used. Consequently, the resulting autocorrelation functions were analyzed using a model taking into account photobleaching, as well as two diffusing components and the presence of a photophysics term (see Analysis of autocorrelation functions) and returning in particular the amplitude of the diffusive term of the autocorrelation function ($G(0)$), the characteristic times associated with the transit of fast and slow molecules through the detection volume (τ_f and τ_s), and the fraction of slow molecules (f). For each measurement, characteristic times were turned into diffusion coefficients using $D = w_0^2/(4\tau)$, after which an effective diffusion coefficient was calculated as $D_{eff} = (1-f)\ D_f + f\ D_s$.

For each series of FCS measurements, the amplitude of the autocorrelation function, $G(0)$, was plotted as a function of the average fluorescence signal (I) and was fit to obtain the molecular brightness (B) of the fluorescent Cic molecules, and the average background noise (I_B) at this position in the embryo, using the expected dependence:

$$G(0) = (B / \gamma)(I - I_B) / I^2,$$

where $\gamma = 2^{3/2}$ is a geometrical factor. Multiple measurements over several days showed that $B = 5.1 \pm 1.4$ kHz and $I_B = 13 \pm 2$ kHz in the conditions of our experiments. Confocal images (typically acquired with pixel size of $d = 0.2$ μm and pixel dwell time of $\delta = 1$ ms) were first adjusted for uneven illumination using a reference image acquired in a fluorophore solution, then each pixel intensity (i) was turned into a concentration (c) using $c = (i / \delta - I_B)/((B/\mathrm{g})\,V)$. The software ilastik was then used to segment all nuclei in the field of view and obtain their average Cic concentration.

Analysis of autocorrelation functions

General form of the autocorrelation functions: The autocorrelation functions, $G(\tau)$, obtained as a result of FCS experiments in embryos expressing Cic-sfGFP were fitted with a model accounting for two mobile components. For commodity these components were assumed to be both diffusive (an assumption commonly made when analyzing FCS data of nuclear proteins).[48-50] An additional term, $G_P(\tau)$, was included in the model, in order to take into account the severe photobleaching that was observed during experiments (even though a low 20 μW excitation intensity, and experiment times as short as 5 s, were used). The function used to fit the data was:

$$G(\tau) = G(0)\left(1 + \frac{T}{1-T}e^{-\tau/\tau_T}\right)\left(\frac{f}{(1+\tau/\tau_f)\left(1+\tau/\left(S^2\tau_f\right)\right)^{1/2}} + \frac{1-f}{(1+\tau/\tau_s)\left(1+\tau/\left(S^2\tau_s\right)\right)^{1/2}}\right) + G_P(\tau) \quad \text{(Equation 1)}$$

When fitting the data, the value of the aspect ratio of the confocal detection volume was fixed to the value determined during calibration experiments, $S = 7$. All other parameters were left free to vary. The mobility of the proteins is characterized by the characteristic times associated with fast proteins (τ_f) and slow proteins (τ_s), and the fraction of fast proteins (f). Diffusion coefficients can be calculated from these characteristic times using $D_{s,f} = w^2/(4\tau_{s,f})$. The value of the $1/e^2$ radius of the confocal detection volume, $w = 301 \pm 7$nm, was determined in calibration experiments involving the diffusion of the fluorophore Alexa 488, which has a known diffusion coefficient $D = 435 \sim \mu m^2/s$.[47] The diffusive part of the correlation function also accounts for the presence of a small but noticeable photophysics term for the sfGFP fluorophore, with a fraction T of dark molecules, and a relaxation time τ_T for the dark state.[51]

Photobleaching: Although photobleaching occurred too slowly to interfere with the measurement of the diffusion characteristic time, it caused a regular decrease in the number of observed fluorescent molecules in the nucleus under study. This translated in a slow change in the average fluorescence signal, I, that could be well approximated by a decaying exponential with characteristic decay time τ_P on the order of the duration of the experiments ($t_M \approx 10$s). Because this characteristic time is well-separated from the other characteristic times in the system (τ_T, τ_f and τ_s), this slow decay in the fluorescence results in a separate term in the correlation which can be well-approximated by:[52]

$$G_P(\tau) = \frac{t_M - \tau}{2\tau_P}\coth\left[\frac{t_M - \tau}{2\tau_P}\right] - 1 \qquad \text{(Equation 2)}$$

Amplitude of the autocorrelation functions: In the absence of background noise, the amplitude of the diffusive part of the correlation function takes the simple form $G(0) = 1 / N$, where N is the average number of fluorescent molecules present in the confocal detection volume, $V = \pi^{3/2} S w^3$. However, experiments in embryos are characterized by a fair amount of background fluorescence, especially after several measurements have already been taken in a particular nucleus and photobleaching has reduced the number of fluorescent proteins. In the presence of background noise with average value I_B, the amplitude of the diffusive part of the correlation function takes the modified form[53,54]

$$G(0) = \frac{1}{N}\frac{1}{(1 + I_B / [I - I_B])^2} \qquad \text{(Equation 3)}$$

Concentration measurements: In the absence of background noise and photobleaching, measuring $G(0)$ leads to a straightforward measurement of the absolute concentration of the fluorophore under study, $c = N/V = 1 /(VG(0))$. However, since the value of $G(0)$ is affected by noise (Equation 3) when working in embryos determining I_B is important. In addition, $G(0)$ reflects only the concentration of visible fluorophores, which in our case was severely affected by photobleaching even after a single short FCS measurement. We thus decided to calculate concentration instead from the pixel intensity measured from images acquired before performing any FCS experiment.

The signal intensity (whether it is the pixel intensity in the image, or the average signal intensity of an FCS measurement, since both were acquired with the same instrument), I, is directly related to the average number of observed fluorophores, N, through:

$$I = \frac{B}{\gamma}N + I_B \qquad \text{(Equation 4)}$$

where B is the effective molecular brightness of the fluorescent protein.

Combining Equations 3 and 4 shows that there is a direct relationship between $G(0)$ and I:

$$G(0) = \frac{B}{\gamma} \times \frac{I - I_B}{I^2} \quad \text{(Equation 5)}$$

If the number of fluorescent proteins, and therefore I, can be made to vary, as is the case in the presence of photobleaching, successive FCS measurements can be used to measure $G(0)$ as a function of I, and fitting this data with the above equation then allows retrieving both B and I_B. Equation 4 can then be used to measure N (either at the pixel of a confocal image or the location of an FCS experiment) and subsequently the absolute fluorophore concentration, c, at that location.

Generation of transgenic flies: Cic-sfGFP generation is described in Keenan et al.[20]

Optimized psMEK: The psMEK1tight construct is available at Addgene plasmid #89361. The optimizing E203K substitution was made by changing the GGA codon to AAG. The construct was assembled into pTIGER as described previously[22] and integrated into the second chromosome using the phiC31 integration system at the attP site and balanced with CyO by The BestGene.

*tll** MS2. Described in Keenan et al.[20]

Endogenous hkb MS2: For insertion of MS2 stem loops into the 5′ UTR of the *hkb* locus, pU6-BbsI-chiRNA expression plasmid[44] and pHD-dsRed-24xMS2 donor plasmid (gifted by the Levine Lab) were coinjected to yw;nos-Cas9(II-attP40) embryos. Microinjection was performed by BestGene. dsRed was used for subsequent screening.

To generate the guide for a cut in the 5′ UTR of *hkb*, two DNA oligos, 5′ CTTCGCGACACTAAATCACTTGGA 3′ and 5′ AAACTCCAAGTGATTTAGTGTCGC 3′, were annealed and inserted into pU6-BbsI-chiRNA plasmid using BbsI sites.

To insert homology arms into the pHD_dsRed_24MS2 plasmid (for homology directed repair), we first amplified the 1000 bp 5′ homology arm of *hkb* from genomic DNA of OreR flies using two primers, cccttcgctgaagcaggtggGCCAGTAAAGTTTTTCTCAAGCACC and agtgcatatgtccgcggccgGGATGGAACACTTGTGATTATGATTTTG. These primers contain overhangs that over lap with the pHD_dsRED_24xMS2 plasmid. The pHD_dsRED_24xMS2 plasmid was linearized by cutting with EcoRI-HF and NheI-HF restriction enzymes (Upstream of the MS2 loops). The 5′ homology arm of *hkb* was then inserted into the plasmid using NEB HiFi assembly master mix. Subsequently, the 1000 bp 3′ homology arm of *hkb* was amplified from genomic DNA using two primers, tacgaagttata gaagagcaAAGTGATTTAGTGTCGCGAGAGAGC and gagcctcgagctgcagaaggGTATGAGTACATGGGCACGAAGATG. The pHD_dsRED_5′Arm_24xMS2 was linearized by cutting with SpeI and StuI restriction enzymes (downstream of the MS2 loops and the dsRED). The 3′ homology arm was then inserted into the plasmid using NEB HiFi assembly master mix.

The dsRED marker is flanked by loxP sites. To remove the dsRED marker from the locus, *hkb*-24xMS2-dsRED flies were crossed to Crey;+;D/Tm3 flies (Bloomington Stock 851). After screening for removal of dsRED, the Crey allele was crossed-out of the final stock.

Modified bnk reporters: All modifications were made from a *bnk* MS2 reporter gerenated in the Rushlow lab. A 130 bp fragment was inserted at the EagI site via in-fusion cloning upstream of the bnk enhancer and promoter driving MS2v7 loops from.[32] The fragment contained “TGAATGAA” for the Cic binding sites. “TGAAGCTA” was used for the mutated Cic binding sites. The fragment inserted at the EagI site to generate the modified reporter with 0 Cic sites was 5′-ttcgtttaaacggccgTGAAGCTATATCTATGATCACTAGTCTCGTGAAGCTAATGTCAGGAGATCTCCAGTTTATGAAGCTATTTACTAAATGAGCTCAGTCGTGAAGCTAcggccggccagatcca-3′. The fragment inserted at the EagI site to generate the modified reporter with 1 Cic site was 5′-ttcgtttaaacggccgTGAAGCTATATCTATGATCACTAGTCTCGTGAAGCTAATGTCAGGAGATCTCCAGTTTATGAAGCTATTTACTAAATGAGCTCAGTCGtgaatgaacggccggccagatcca-3′. The fragment inserted at the EagI site to generate the modified reporter with 4 Cic sites was 5′-ttcgtttaaacggccgtgaatgaaTATCTATGATCACTAGTCTCGtgaatgaaATGTCAGGAGATCTCCAGTTTAtgaatgaaTTTACTAAATGAGCTCAGTCGtgaatgaacggccggccagatcca-3′. These fragments were designed from a region of a synthetic Cic-responsive construct courtesy of Nareg Djabrayan and the Jimenez lab. The construct was integrated into the 3rd chromosome using the phiC31 system by BestGene Inc (line #9750).

Combining optimized psMEK, MCP-mCherry, and MS2 reporters—The optimized psMEK transgenic flies were double balanced with Sp/Cyo ; Dr/Tm3 and crossed with MCP-mCherry on the third chromosome to generate optimized psMEK ; MCP-mCherry. P(matα-GAL-VP16)mat67; P(matα-GAL-VP16)mat15 was crossed with Sp/Cyo ; Dr/Tm3 to generate P(matα-GAL-VP16)mat67; Dr/Tm3, which was crossed with miFP-Histone on the third chromosome. Virgin females with P(matα-GAL-VP16)mat67 driving optimized psMEK expression and expressing MCP-mCherry were placed in a cage with MS2 reporter males for the experimental cross generating embryos to be imaged. The miFP-Histone was not used in this study.

Optogenetic illumination and live imaging—Embryos were collected on a yeasted apple juice plate in a cage placed in an aluminum foil-lined box under a 505 nm LED panel made in-house, described in Patel et al.[22] The T4 3/4 LEDs were purchased from https://www.superbrightleds.com/. Voltage was supplied by the KORAD KA3005D power supply from amazon.com. Embryos were collected for 1-2 hours under light. Embryos that did not have visible pole cells, which were visualized in halocarbonoil on the collection plate, were manually dechorionated, and mounted on their lateral side in a live imaging chamber consisting of a gas permeable membrane with halocarbon oil and a coverslip. All imaging was performed on a Leica SP5 point scanning confocal microscope. Embryos were illuminated with 10% 488 nm laser to activate optimized photoswitchable MEK and to image the cytoplasmic Dronpa fluorescent signal. 10% 405 nm laser was used to inactivate

embryos. Embryos were staged by the density of apparent nuclei at the surface. The 561 nm laser was used to image the MCP-mCherry fluorescent signal. For *tll**MS2, the 63x objective was used and pinhole was also opened to 1.6 AU. 12.65 μm stacks with 0.55 μm steps were taken every 29 s with an imaging frequency of 400 Hz. For *hkb* and *bnk* + 4cic, the 63x objective was used and zoomed to 2.5x. Imaging frequency was 700 Hz. 14.77μm stacks with 0.67 μm steps were taken every 17 s, and 15% 515nm laser was used to activate the optogenetic tool.

Quantification of percent nuclei transcribing—Max projections of the mCherry channel were made in FIJI[45] for all movies. A Gaussian blur with a radius of 4 was applied to the max projection and then subtracted from the original max projection. The image sequences of background subtracted max projections were processed in MATLAB to count the number of MS2 dots. The open source FastPeakFind MATLAB function with a user supplied threshold was used to count the number of dots at each time point. The total number of nuclei was counted by inverting the image from the Dronpa channel (cytoplasmic Dronpa outlines nuclei) and using imfindcircles in MATLAB. The % nuclei transcribing was calculated by dividing the number of dots detected per frame by the number of nuclei for the embryo counted from the middle slice of the z stack immediately before the 488 nm laser was switched off.

Spot detection of transcriptional bursts—The spot detection algorithm in the imaging software Imaris was used. Spots detection parameters were as follows: 1 μm for hkb and 1.5 μm for *bnk* + 4 cic, user specified intensity standard deviation threshold above the noise, maximum distance 3 μm and no allowed gap size. Autoregressive motion was selected for spot tracking. For the intensity traces of example tracked spots in Figure 3, a maximum gap distance of the number of frames was allowed, and gaps were filled with all detected objects. Spot intensity means were normalized by the intensity of the cytoplasmic mCherry signal from the time frame at the start of nc 14. Intensity was measured in FIJI, from a reconstructed image exported from Imaris. All images exported had consistent parameters in the Display Adjustment window before measuring intensity in FIJI.

Burst initiation time—The burst initiation time was defined as the time after the photoswitch from activating to inactivating light at which the individually tracked spot was first detected.

QUANTIFICATION AND STATISTICAL ANALYSIS

Quantification of transcription activity—The mean and standard deviations of the percent nuclei transcribing were calculated in MATLAB. 2-sample Kolmogorov-Smirnov tests (two-tailed) from the scipy.stats package in Python were used to calculate the KS-test statistics and p values of the spot lifetimes and peak intensities. For the *hkb* reporter, the numbers of de-repressed and repressed bursts were 298 (from 2 embryos) and 340 (from 3 embryos) respectively. For the *bnk* + 4cic reporter, the numbers of de-repressed and repressed bursts were 220 (from 2 embryos) and 106 (from 2 embryos) respectively. Truncated violin plots show the median and quartiles with thick and thin lines respectively.

Box and whisker plots with Tukey whiskers generated in GraphPad Prism 9 are shown to represent the burst initiation times.

Supplementary Material

Refer to Web version on PubMed Central for supplementary material.

ACKNOWLEDGMENTS

We thank Shigehiro Yamada and Mengyu Li for the *bnk* MS2 reporter plasmid and Nareg Djabrayan for the synthetic Cic-responsive MS2 reporter sequence. We also thank Lucy Reading-Ikkanda for graphic design of the figures. We also thank Daniel Larson, Ido Golding, Mike Levine, Nicholas Treen, Gertrud Schüpbach, and Eric Wieschaus for helpful discussions. The research was supported by National Institutes of Health (NIH) research grants, DP2EB024247, F32GM119297, RO1HD0858870, and HD085870 to S.Y.S. and RO1GM63024 to C.A.R., and by Natural Sciences and Engineering Research Council of Canada (NSERC) grant RGPIN-2015-06362 to C.F.

REFERENCES

1. Kim JW, Ponce RK, and Okimoto RA (2021). Capicua in human cancer. Trends Cancer 7, 77–86. [PubMed: 32978089]
2. Lee Y (2020). Regulation and function of capicua in mammals. Exp. Mol. Med 52, 531–537. [PubMed: 32238859]
3. Jiménez G, Guichet A, Ephrussi A, and Casanova J (2000). Relief of gene repression by torso RTK signaling: role of capicua in Drosophila terminal and dorsoventral patterning. Genes Dev. 14, 224–231. [PubMed: 10652276]
4. Gaston K, and Jayaraman PS (2003). Transcriptional repression in eukaryotes: repressors and repression mechanisms. Cell. Mol. Life Sci 60, 721–741. [PubMed: 12785719]
5. Patel AL, and Shvartsman SY (2018). Outstanding questions in developmental ERK signaling. Development 145, dev143818. [PubMed: 30049820]
6. Reynolds N, O'Shaughnessy A, and Hendrich B (2013). Transcriptional repressors: multifaceted regulators of gene expression. Development 140, 505–512. [PubMed: 23293282]
7. Bunda S, Heir P, Metcalf J, Li ASC, Agnihotri S, Pusch S, Yasin M, Li M, Burrell K, Mansouri S, et al. (2019). CIC protein instability contributes to tumorigenesis in glioblastoma. Nat. Commun 10, 661. [PubMed: 30737375]
8. Lee H, and Song JJ (2019). The crystal structure of Capicua HMG-box domain complexed with the ETV5-DNA and its implications for Capicua-mediated cancers. FEBS J 286, 4951–4963. [PubMed: 31323153]
9. Ajuria L, Nieva C, Winkler C, Kuo D, Samper N, Andreu MJ, Helman A, González-Crespo S, Paroush Z, Courey AJ, and Jiménez G (2011). Capicua DNA-binding sites are general response elements for RTK signaling in Drosophila. Development 138, 915–924. [PubMed: 21270056]
10. Cinnamon E, Helman A, Ben-Haroush Schyr R, Orian A, Jiménez G, and Paroush Z (2008). Multiple RTK pathways downregulate Groucho-mediated repression in Drosophila embryogenesis. Development 135, 829–837. [PubMed: 18216172]
11. Jiménez G, Shvartsman SY, and Paroush Z (2012). The Capicua repressor–a general sensor of RTK signaling in development and disease. J. Cell Sci 125, 1383–1391. [PubMed: 22526417]
12. Lee JS, Kim E, Lee J, Kim D, Kim H, Kim CJ, Kim S, Jeong D, and Lee Y (2020). Capicua suppresses colorectal cancer progression via repression of ETV4 expression. Cancer Cell Int. 20, 42. [PubMed: 32042269]
13. Lemmon MA, and Schlessinger J (2010). Cell signaling by receptor tyrosine kinases. Cell 141, 1117–1134. [PubMed: 20602996]
14. Goyal Y, Schüpbach T, and Shvartsman SY (2018). A quantitative model of developmental RTK signaling. Dev. Biol 442, 80–86. [PubMed: 30026122]

15. Pignoni F, Baldarelli RM, Steingrímsson E, Diaz RJ, Patapoutian A, Merriam JR, and Lengyel JA (1990). The Drosophila gene tailless is expressed at the embryonic termini and is a member of the steroid receptor superfamily. Cell 62, 151–163. [PubMed: 2364433]
16. Brönner G, and Jäckle H (1996). Regulation and function of the terminal gap gene huckebein in the Drosophila blastoderm. Int. J. Dev. Biol 40, 157–165. [PubMed: 8735925]
17. Goldstein RE, Jiménez G, Cook O, Gur D, and Paroush Z (1999). Huckebein repressor activity in Drosophila terminal patterning is mediated by Groucho. Development 126, 3747–3755. [PubMed: 10433905]
18. Forés M, Simón-Carrasco L, Ajuria L, Samper N, González-Crespo S, Drosten M, Barbacid M, and Jiménez G (2017). A new mode of DNA binding distinguishes Capicua from other HMG-box factors and explains its mutation patterns in cancer. PLoS Genet. 13, e1006622. [PubMed: 28278156]
19. Grimm O, Sanchez Zini V, Kim Y, Casanova J, Shvartsman SY, and Wieschaus E (2012). Torso RTK controls Capicua degradation by changing its subcellular localization. Development 139, 3962–3968. [PubMed: 23048183]
20. Keenan SE, Blythe SA, Marmion RA, Djabrayan NJ, Wieschaus EF, and Shvartsman SY (2020). Rapid dynamics of signal-dependent transcriptional repression by Capicua. Dev. Cell 52, 794–801.e4. [PubMed: 32142631]
21. Zhou XX, Fan LZ, Li P, Shen K, and Lin MZ (2017). Optical control of cell signaling by single-chain photoswitchable kinases. Science 355, 836–842. [PubMed: 28232577]
22. Patel AL, Yeung E, McGuire SE, Wu AY, Toettcher JE, Burdine RD, and Shvartsman SY (2019). Optimizing photoswitchable MEK. Proc. Natl. Acad. Sci. USA 116, 25756–25763. [PubMed: 31796593]
23. Clauß K, Popp AP, Schulze L, Hettich J, Reisser M, Escoter Torres L, Uhlenhaut NH, and Gebhardt JCM (2017). DNA residence time is a regulatory factor of transcription repression. Nucleic Acids Res. 45, 11121–11130. [PubMed: 28977492]
24. Abu-Arish A, Porcher A, Czerwonka A, Dostatni N, and Fradin C (2010). High mobility of bicoid captured by fluorescence correlation spectroscopy: implication for the rapid establishment of its gradient. Biophys. J 99, L33–L35. [PubMed: 20712981]
25. Atkins PW, and De PJ (2002). Atkins' Physical Chemistry (Oxford University).
26. Li X-Y, Thomas S, Sabo PJ, Eisen MB, Stamatoyannopoulos JA, and Biggin MD (2011). The role of chromatin accessibility in directing the widespread, overlapping patterns of Drosophila transcription factor binding. Genome Biol. 12, R34. [PubMed: 21473766]
27. Garcia HG, Tikhonov M, Lin A, and Gregor T (2013). Quantitative imaging of transcription in living Drosophila embryos links polymerase activity to patterning. Curr. Biol 23, 2140–2145. [PubMed: 24139738]
28. Zhou XX, Chung HK, Lam AJ, and Lin MZ (2012). Optical control of protein activity by fluorescent protein domains. Science 338, 810–814. [PubMed: 23139335]
29. Rodriguez J, and Larson DR (2020). Transcription in living cells: molecular mechanisms of bursting. Annu. Rev. Biochem 89, 189–212. [PubMed: 32208766]
30. Tunnacliffe E, and Chubb JR (2020). What is a transcriptional burst? Trends Genet. 36, 288–297. [PubMed: 32035656]
31. Liang HL, Nien CY, Liu HY, Metzstein MM, Kirov N, and Rushlow C (2008). The zinc-finger protein Zelda is a key activator of the early zygotic genome in Drosophila. Nature 456, 400–403. [PubMed: 18931655]
32. Yamada S, Whitney PH, Huang SK, Eck EC, Garcia HG, and Rushlow CA (2019). The Drosophila pioneer factor Zelda modulates the nuclear microenvironment of a dorsal target enhancer to potentiate transcriptional output. Curr. Biol 29, 1387–1393.e5. [PubMed: 30982648]
33. Bartman CR, Hamagami N, Keller CA, Giardine B, Hardison RC, Blobel GA, and Raj A (2019). Transcriptional burst initiation and polymerase pause release are key control points of transcriptional regulation. Mol. Cell 73, 519–532.e4. [PubMed: 30554946]
34. Fukaya T, Lim B, and Levine M (2017). Rapid rates of Pol II elongation in the Drosophila embryo. Curr. Biol 27, 1387–1391. [PubMed: 28457866]

35. Bothma JP, Magliocco J, and Levine M (2011). The snail repressor inhibits release, not elongation, of paused Pol II in the Drosophila embryo. Curr. Biol 21, 1571–1577. [PubMed: 21920753]
36. Soutourina J (2018). Transcription regulation by the Mediator complex. Nat. Rev. Mol. Cell Biol 19, 262–274. [PubMed: 29209056]
37. Fukaya T, Lim B, and Levine M (2016). Enhancer control of transcriptional bursting. Cell 166, 358–368. [PubMed: 27293191]
38. Zaborowska J, Egloff S, and Murphy S (2016). The pol II CTD: new twists in the tail. Nat. Struct. Mol. Biol 23, 771–777. [PubMed: 27605205]
39. Shao W, and Zeitlinger J (2017). Paused RNA polymerase II inhibits new transcriptional initiation. Nat. Genet 49, 1045–1051. [PubMed: 28504701]
40. Chambers M, Turki-Judeh W, Kim MW, Chen K, Gallaher SD, and Courey AJ (2017). Mechanisms of Groucho-mediated repression revealed by genome-wide analysis of Groucho binding and activity. BMC Genomics 18, 215. [PubMed: 28245789]
41. Weissmann S, Cloos PA, Sidoli S, Jensen ON, Pollard S, and Helin K (2018). The tumor suppressor CIC directly regulates MAPK pathway genes via histone deacetylation. Cancer Res. 78, 4114–4125. [PubMed: 29844126]
42. Liang Z, Brown KE, Carroll T, Taylor B, Vidal IF, Hendrich B, Rueda D, Fisher AG, and Merkenschlager M (2017). A high-resolution map of transcriptional repression. eLife 6, 1–24.
43. Hunter C, and Wieschaus E (2000). Regulated expression of nullo is required for the formation of distinct apical and basal adherens junctions in the Drosophila blastoderm. J. Cell Biol 150, 391–401. [PubMed: 10908580]
44. Gratz SJ, Wildonger J, Harrison MM, and O'Connor-Giles KM (2013). CRISPR/Cas9-mediated genome engineering and the promise of designer flies on demand. Fly (Austin) 7, 249–255. [PubMed: 24088745]
45. Schindelin J, Arganda-Carreras I, Frise E, Kaynig V, Longair M, Pietzsch T, Preibisch S, Rueden C, Saalfeld S, Schmid B, et al. (2012). Fiji: an open-source platform for biological-image analysis. Nat. Methods 9, 676–682. [PubMed: 22743772]
46. Pédelacq J-D, Cabantous S, Tran T, Terwilliger TC, and Waldo GS (2006). Engineering and characterization of a superfolder green fluorescent protein. Nat. Biotechnol 24, 79–88. [PubMed: 16369541]
47. Petrásek Z, and Schwille P (2008). Precise measurement of diffusion coefficients using scanning fluorescence correlation spectroscopy. Biophys. J 94, 1437–1448. [PubMed: 17933881]
48. Wachsmuth M, Waldeck W, and Langowski J (2000). Anomalous diffusion of fluorescent probes inside living cell nuclei investigated by spatially-resolved fluorescence correlation spectroscopy. J. Mol. Biol 298, 677–689. [PubMed: 10788329]
49. Porcher A, Abu-Arish A, Huart S, Roelens B, Fradin C, and Dostatni N (2010). The time to measure positional information: maternal hunchback is required for the synchrony of the Bicoid transcriptional response at the onset of zygotic transcription. Development 137, 2795–2804. [PubMed: 20663819]
50. Vukojevic V, Papadopoulos DK, Terenius L, Gehring WJ, and Rigler R (2010). Quantitative study of synthetic Hox transcription factor-DNA interactions in live cells. Proc. Natl. Acad. Sci. USA 107, 4093–4098. [PubMed: 20147625]
51. Widengren J, Mets U, and Rigler R (1995). Fluorescence correlation spectroscopy of triplet states in solution: A theoretical and experimental study. J. Phys. Chem 99, 13368–13379.
52. Bacia K (2005). Dynamic processes in membranes studied by fluorescence correlation spectroscopy. PhD thesis (Technische Universität Dresden).
53. Koppel DE (1974). Statistical accuracy in fluorescence correlation spectroscopy. Phys. Rev. A 10, 1938–1945.
54. Rigler R, Mets U, Widengren J, and Kask P (1993). Fluorescence correlation spectroscopy with high count rate and low background: analysis of translational diffusion. Eur. Biophys. J 22, 169–175.

Highlights

- Fluorescence correlation spectroscopy measurements estimate Capicua search time
- Optimized photoswitchable MEK provides direct and reversible Capicua control
- Transcription halts minutes after removing optogenetic signals antagonizing Capicua
- Gene repression by Capicua interferes with the emergence of transcriptional bursts

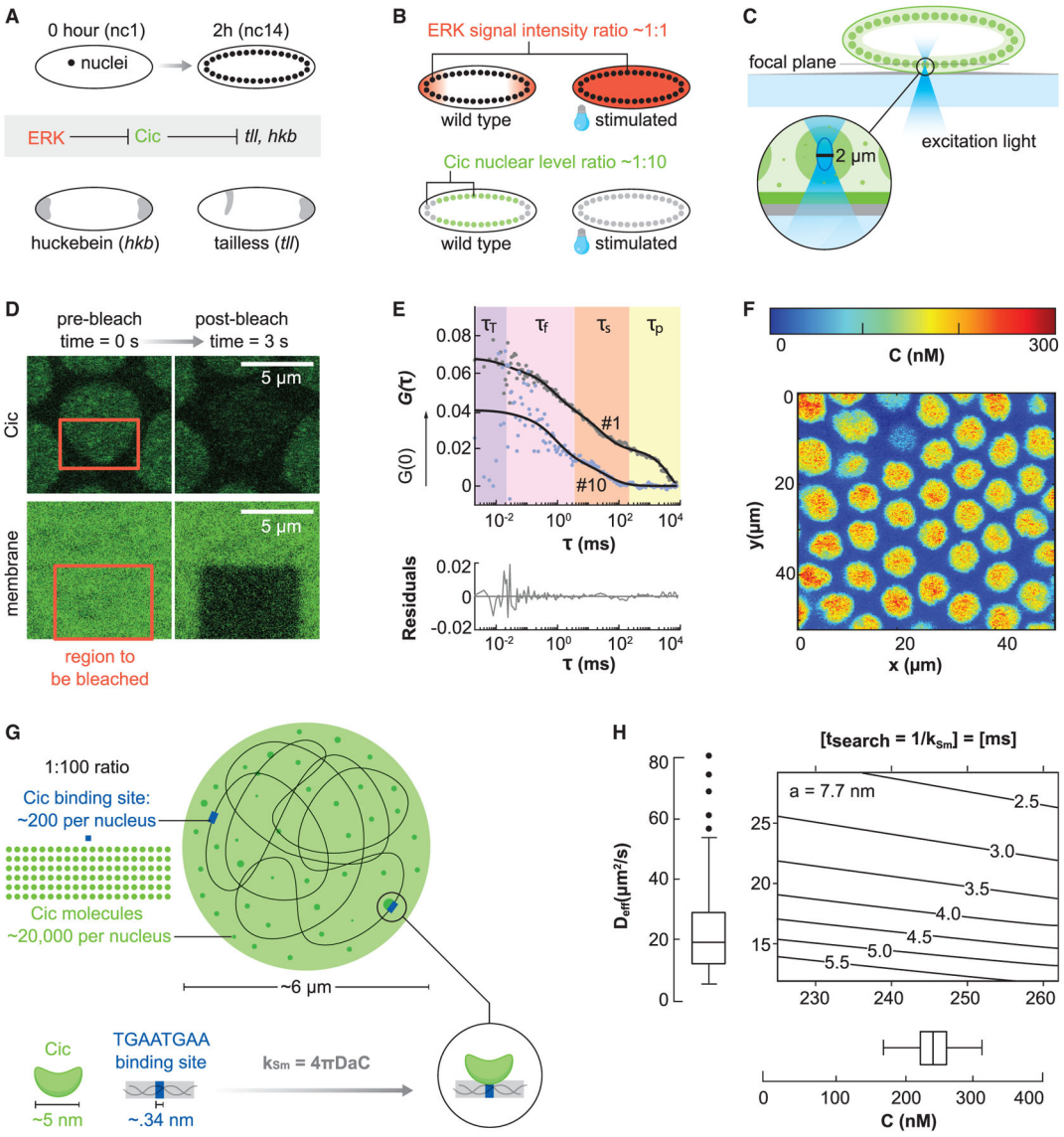

Figure 1. Measurements of Cic concentration and mobility in interphase nuclei

(A) 13 synchronous nuclear divisions (14 nuclear cycles, “nc”) take place in a shared cytoplasm during the first 2 h of embryogenesis. The nuclei migrate to the periphery of the embryo, forming a uniform layer. In this time window, active ERK (red) signals antagonize Cic (green), a transcription factor that represses expression of the genes *tailless* (*tll*) and *huckebein* (*hkb*). Wild-type expression domains of *tll* and *hkb* are shown in gray.

(B) ERK is endogenously active at the poles (shown in red). Illuminating embryos expressing the optogenetic signaling tool optimized photoswitchable MEK activates ERK uniformly in the middle as well as at the poles. Previous quantifications suggest that levels of optogenetically activated ERK in the middle are at least equivalent to the levels at the anterior pole. Cic (green) is de-repressed in the poles of wild-type embryos, where ERK is active. Previous studies reported an ~10-fold reduction of Cic in ERK-activated nuclei at the

poles compared to ERK-free nuclei in the middle. Optogenetic ERK signals that are at least as strong as endogenous ERK signals are expected to also de-repress Cic.

(C) Schematic of the confocal setup used to image Cic endogenously tagged with the fluorescent marker sfGFP in nuclei from the middle of an embryo. The confocal detection volume (dark blue ellipse in the inset) is smaller than a nucleus.

(D) Dynamics of Cic molecules observed via fluorescence recovery after photobleaching (FRAP). Partial bleaching of a nucleus shows that all Cic molecules are mobile on the ~1-s timescale. Photobleaching of the embryo's vitelline membrane (lower panels) demonstrates that the bleach area is visible and well defined for immobile fluorophores. The bleach area is delineated in red. Right panels show the same samples 3 s after the beginning of the photobleaching step.

(E) Dynamics of diffusing Cic molecules as observed by fluorescence correlation spectroscopy (FCS). The first (no. 1) and the last (no. 10) autocorrelation functions in a representative series of 10 successive measurements obtained in a single nucleus are shown. Data (dots) were fit with a model (lines) that includes two diffusing Cic populations (characterized by times τ_f and τ_s), a photobleaching term (relaxation time τ_P), and a photophysics term (relaxation time τ_T). The lower panel shows the residuals of this fit for curve no. 1.

(F) Concentration heatmap calculated from the pixel intensities of a typical confocal image acquired in the middle of a Cic-sfGFP embryo, using the values of the background noise (I_B) and molecular brightness (B) extracted from FCS measurements. The nuclear Cic-sfGFP concentration is uniform among the nuclei in this field of view.

(G) From concentration, the number of Cic molecules per nucleus is estimated to be ~20,000 (assuming nuclei are spherical with a radius of 3 μm). There are ~200 Cic binding loci in the genome from a Cic ChIP-seq study. The measured concentration and diffusivity values are parameters that can be used to estimate the time for a single Cic molecule to search for and find its target region on the DNA. The Smoluchowski equation ($k_{Sm} = 4\pi DaC$) describes this rate constant in terms of diffusivity "D" and concentration "C" as well as a characteristic length scale "a." This length scale can be set by the average size of a protein (5 nm) and an estimate for the size of a base pair (0.34 nm).

(H) A range of search times ($1/k_{Sm}$) based on the Smoluchowski equation are shown (timescale is milliseconds). Box and whisker plots of the values measured for the effective diffusion coefficient (D_{eff}) and concentration (C) of nuclearCic-sfGFP are shown on the y and x axis, respectively. For D_{eff}, each point in the dataset is the result of a single FCS measurement acquired during either nc 13 (30 measurements) or nc 14 (50 measurements), in 8 different nuclei. For C, each point in the dataset represents the average concentration in a single nucleus during early nc 14 (693 nuclei in total). The 25%–75% interval was used in the search time estimation shown in the contour plot. 7.7 nm was used as a fixed length scale "a," the sum of the average size of a protein and the Cic binding site "TGAATGAA" (0.34 nm/bp × 8 bp = 2.7 nm).

See also Figure S1.

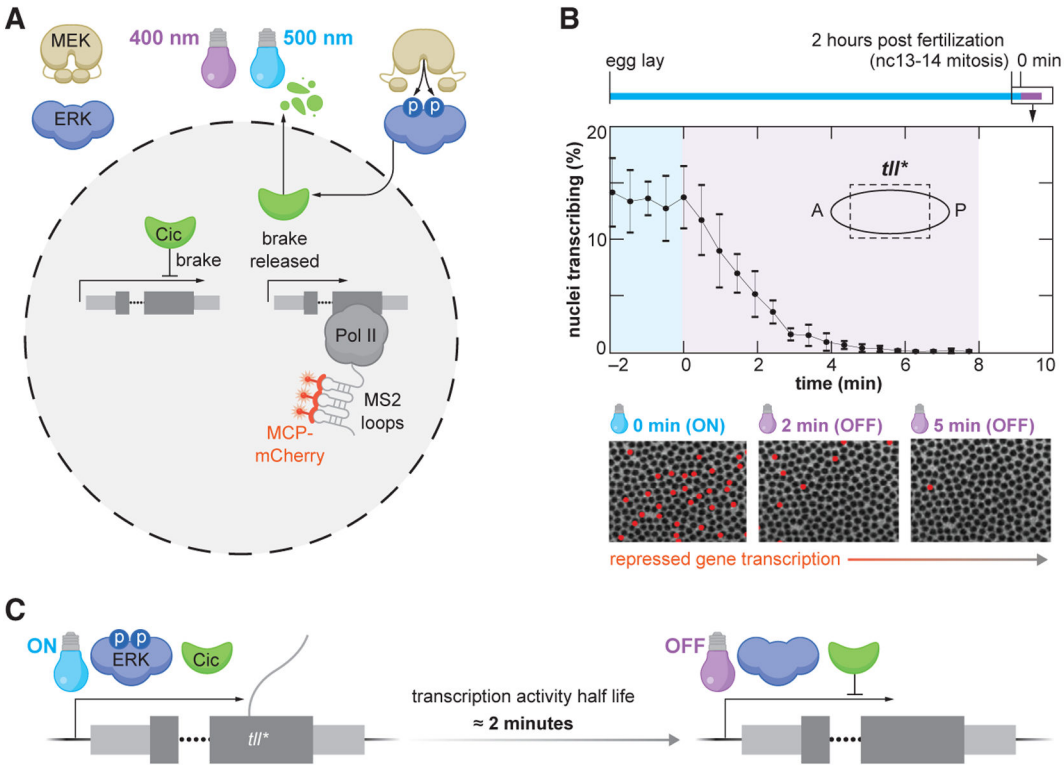

Figure 2. Transcriptional readouts of optogenetic perturbations reveal fast repression by Cic

(A) Optimized photoswitchable MEK (psMEK) reversibly controls phosphorylation (indicated by "P" in blue circles) and activation of ERK. 500-nm light dissociates photo-dimerizable Dronpa domains flanking the active site of MEK containing activating mutations, thereby allowing MEK to access its substrate, ERK. 400 nm illumination dimerizes the domains over the active site of MEK, blocking MEK-ERK interaction. This light-sensitive ERK-activating tool was genetically combined with a transgenic system for reporting live transcription with MS2-MCP reporters. Fluorescently tagged MCP-mCherry (red) binds to MS2 stem loops as RNA polymerase (Pol II) transcribes genes. Altogether, optimized psMEK and the MS2-MCP system enable real-time optogenetic control of the Cic transcriptional brake alongside measurements of the immediate transcriptional responses.

(B) Embryos were illuminated with activating light from the time of egg lay to nc 14, which spans approximately 2 h. Light was switched from activating (blue) to inactivating (purple) 2 min into nc 14, after the completion of the nc 13 to nc 14 mitosis. 0 min marks the time of photoswitching. Percentage of nuclei with a fluorescent dot indicating binding of MCP-mCherry to MS2 loops driven by fragments of the *tll* enhancer (*tll**) in the middle of the embryo are shown. Snapshots from the middle of the embryo at 0, 2, and 5 min after optimized psMEK inactivation are shown with transcriptionally active nuclei marked by red dots. Error bars represent one standard deviation (n = 5 embryos).

(C) The half-life of transcription activity when optimized psMEK is switched off, following long-term activation, is −2 min.

See also Figure S2.

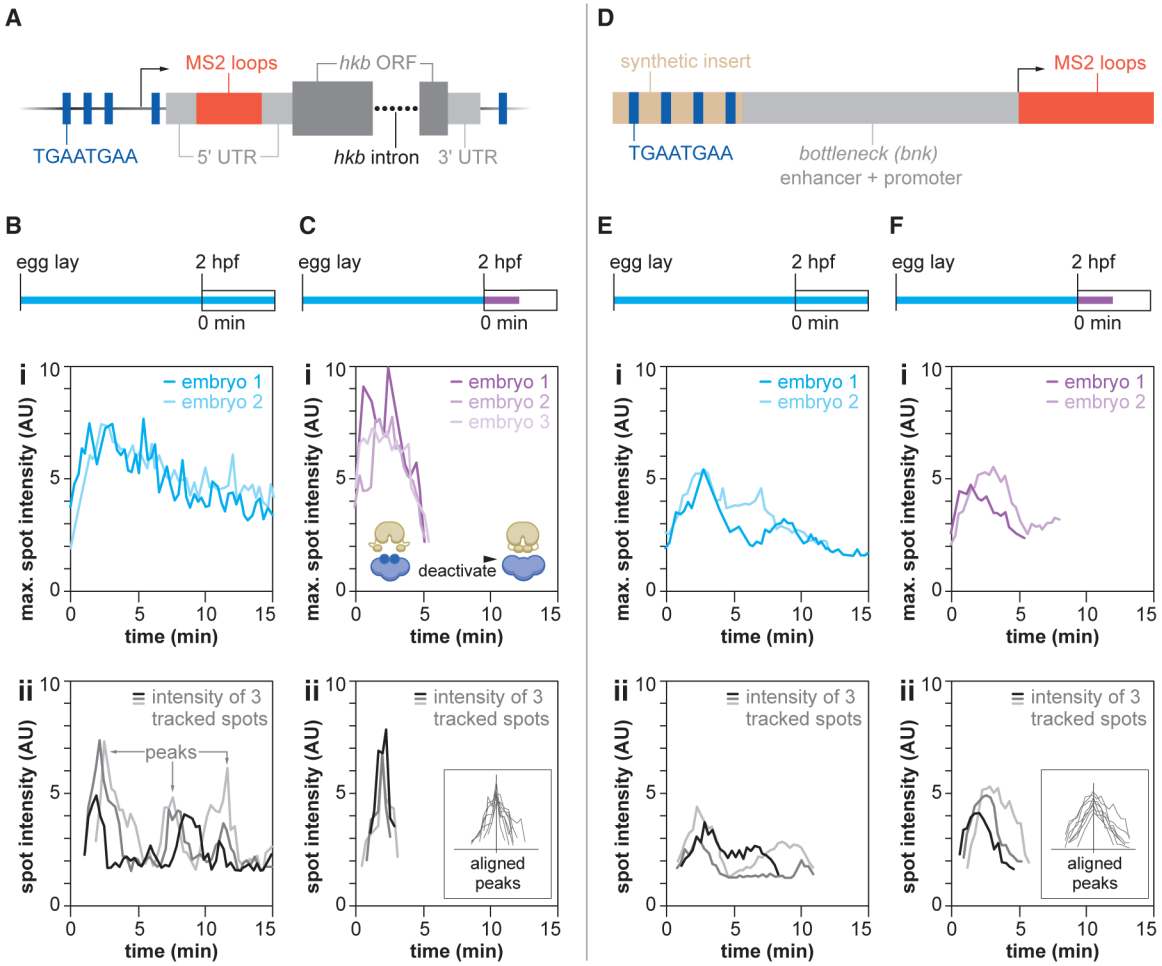

Figure 3. Photoswitching MEK limits the transcriptional bursting time window

(A) MS2 loops were inserted at the endogenous *hkb* locus via CRISPR. Thick dark gray bars designate the open reading frames (ORFs), thin dark gray bars are 3′ or 5′ UTRs, and dotted lines are introns. The *hkb* regulatory region has 5 strong Cic binding sites “TGAATGAA” (blue bars).

(B) Transcription responses in the middle of embryos expressing the endogenous *hkb* reporter and continuously illuminated with light that activates the optogenetic ERK signal. The colored bar represents the optogenetic illumination schedule, and the box represents the data collection time window. Developmental time is indicated above the light schedule. Activating light (blue) was provided from the time of egg lay throughout nc 14. Data collection starts at 0 min, which corresponds to 0 min in each of the plots below. (i) For each time frame, the maximum recorded spot intensity is plotted for 2 embryos. (ii) Examples of intensity time series from 3 individually tracked spots are shown and apparent burst “peaks” are denoted.

(C) Transcription responses in the middle of embryos expressing the endogenous *hkb* reporter and exposed to a change in optogenetic illumination wavelength after the nc 13 to nc 14 mitosis. Activating light (blue) was provided from the time of egg lay to the nc 13 to nc 14 mitosis (~2 hpf). Optogenetic illumination was then immediately switched to

the inactivating wavelength (purple). The data collection time window starts at time of the optogenetic switch. (i) For each time frame, the maximum recorded spot intensity is plotted for 3 embryos. (ii) Examples of intensity time series from 3 individually tracked spots are shown. 10 tracked spots aligned by their maximum intensities are shown in the inset.
(D) ACic-dependent reporter was constructed by inserting four strong Cic binding sites "TGAATGAA" (dark blue) spaced 21 bp apart directly upstream of the *bnk* enhancer and promoter driving MS2 loops.
(E) Transcription responses in the middle of embryos expressing the modified *bnk* reporter and continuously illuminated with the activating light (blue). The optogenetic light schedule was identical to the continuous light schedule for the *hkb* reporter described in (B). (i) Maximum recorded spot intensity per time frame for 2 embryos is shown. (ii) Example intensity time series from 3 individually tracked spots is shown.
(F) Transcription responses in the middle of embryos expressing the modified *bnk* reporter and exposed to a change in optogenetic illumination wavelength after the nc 13 to nc 14 mitosis. The optogenetic light schedule was identical to the photoswitched light schedule for the *hkb* reporter described in (C). (i) The maximum recorded spot intensity per time frame for 2 embryos is plotted. (ii) Example intensity time series from 3 individually tracked spots is shown, with 10 time series aligned by maximum intensity in the inset.
See also Figure S3.

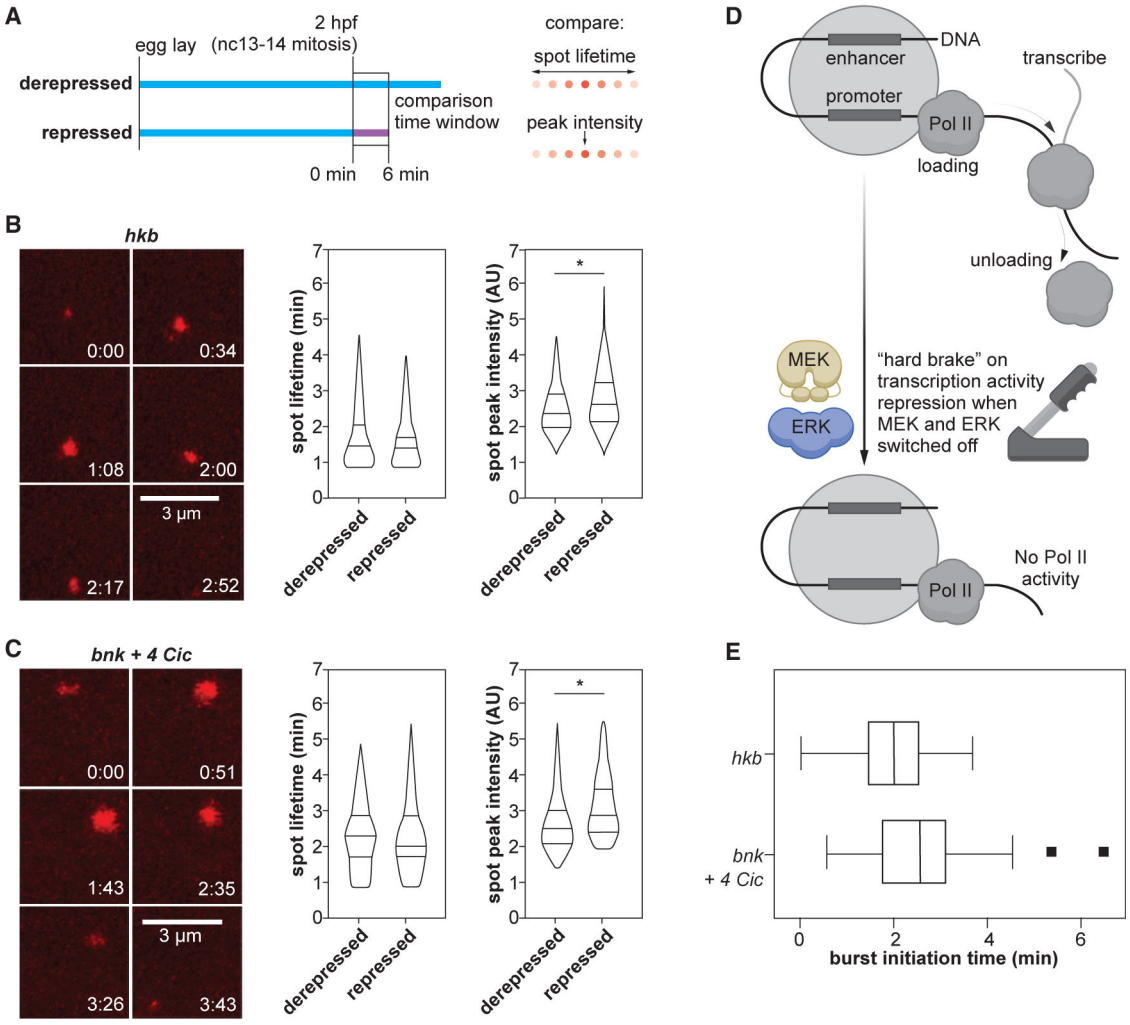

Figure 4. Repressed and de-repressed bursts are similar

(A) Tracked spots representing apparent transcriptional bursts were considered from the first 6 min of movies taken from embryos that were subject repression by Cic (optimized psMEK switched off at 0 min, purple) or de-repressed (continuous optimized psMEK activation, blue).

(B) Tracked spots were pooled for the de-repressed and repressed optogenetic conditions, respectively, from embryos expressing the *hkb* reporter. The lifetimes and peak intensities of the tracked spots for each condition are shown. The distributions of these values are displayed as truncated violin plots, with the median and quartiles represented (horizontal lines). *$p < 0.05$ for a 2-sample Kolmogorov-Smirnov test (KS test statistic for spot lifetimes = 0.094; KS test statistic for spot peak intensities = 0.161). Pooled numbers of spots used to generate the distributions were $n_{\text{de-repressed}} = 298$ and $n_{\text{repressed}} = 340$.

(C) Tracked spots were pooled for the de-repressed and repressed optogenetic conditions, respectively, from embryos expressing the modified *bnk* + 4 Cic sites reporter. The distributions of the spot lifetimes and peak intensities for each condition are shown. *$p < 0.05$ for a 2-sample Kolmogorov-Smirnov test (KS test statistic for spot lifetimes = 0.078;

KS test statistic for spot peak intensities = 0.251). Pooled numbers of spots used to generate the distributions were $n_{de\text{-}repressed}$ = 220 and $n_{repressed}$ = 106.

(D) A “hard brake” on ERK signaling enabled by photoswitching MEK leads to severely interrupted transcription burst generation of Cic-responsive target genes. A hard brake on transcription may involve multiple factors that interact with enhancers and promoters and would prevent polymerase activity from being initiated.

(E) Box and whisker plots of the apparent burst initiation times, defined as the time it takes for a spot to be first detected after switching optimized psMEK off at the start of nc 14, for the *hkb* and *bnk* + 4 Cic sites reporters.

See also Figure S4.

KEY RESOURCES TABLE

REAGENT or RESOURCE	SOURCE	IDENTIFIER
Experimental models: organisms/strains		
Drosophila melanogaster. UAS-psMEKE203K	Patel et al.[22]	N/A
Drosophila melanogaster. MCP-mCherry	Levine lab	N/A
Drosophila melanogaster. *tll*-MS2	Keenan et al.[20]	N/A
Drosophila melanogaster. *Hkb*-MS2	This study	N/A
Drosophila melanogaster. *Bnk*+4Cic-MS2	This Study	N/A
Drosophila melanogaster. P(matα-GAL-VP16)mat67; P(matα-GAL-VP16)mat15	Hunter and Wieschaus[43]	N/A
Drosophila melanogaster. Sp/Cyo ; Dr/Tm3	N/A	N/A
Drosophila melanogaster. Crey;+;D/Tm3	Bloomington Stock 851	RRID: BDSC_851
Drosophila melanogaster. *CicsfGFP*	Keenan et al.[20]	N/A
Oligonucleotides		
4 Cic sites insert to *bnk*-MS2, 5′-ttcgtttaaacggccgtgaatgaaTATCTATGATCACTAGTCTCG tgaatgaaATGTCAGGAGATCTCCAGTTTAtgaatgaaTTTAC TAAATGAGCTCAGTCGtgaatgaacggccggccagatcca-3′	This paper	N/A
1 Cic site insert to *bnk*-MS2, 5′-ttcgtttaaacggccgTGAAG CTATATCTATGATCACTAGTCTCGTGAAGCTAATGTCA GGAGATCTCCAGTTTATGAAGCTATTTACTAAATGAGC TCAGTCGtgaatgaacggccggccagatcca-3′	This paper	N/A
0 Cic site insert to *bnk*-MS2, 5′-ttcgtttaaacggccgTGAAGCTATATCTATGATCACTAGTCTCGTGAAGCTAATGTCA GGAGATCTCCAGTTTATGAAGCTATTTACTAAATGAGC TCAGTCGTGAAGCTAcggccggccagatcca-3′	This paper	N/A
Guide for *hkb* reporter CRISPR, 5′ CTTCGCGACACTAAATCACTTGGA 3′	This paper	N/A
Guide for *hkb* reporter CRISPR, 5′ AAACTCCAAGTGATTTAGTGTCGC 3′	This paper	N/A
5′ homology arm of *hkb* amplification, agtgcatatgt ccgcggccgGGATGGAACACTTGTGATTATGATTTTG	This paper	N/A
5′ homology arm of *hkb* amplification, cccttcgct gaagcaggtggGCCAGTAAAGTTTTTCTCAAGCACC	This paper	N/A
3′ homology arm of *hkb* amplification, tacgaagttata gaagagcaAAGTGATTTAGTGTCGCGAGAGAGC	This paper	N/A
3′ homology arm of *hkb* amplification, gagcctcgag ctgcagaaggGTATGAGTACATGGGCACGAAGATG	This paper	N/A
Recombinant DNA		
pb-phi-bnkMS2	Rushlow lab	N/A
pU6-BbsI-chiRNA	Gratz et al.[44]	RRID: Addgene_45946
pHD-dsRed-24xMS2	Levine lab	N/A
Software and algorithms		
Imaris	https://imaris.oxinst.com/packages	RRID: SCR_007370
FIJI	Schindelin et al.[45]	RRID: SCR_002285
Python	https://www.python.org/	RRID: SCR_008394

REAGENT or RESOURCE	SOURCE	IDENTIFIER
MATLAB	https://www.mathworks.com/products/matlab/	RRID: SCR_001622
GraphPad Prism 9	https://www.graphpad.com:443/	RRID: SCR_002798
Ilastik	https://ilastik.org/	RRID: SCR_015246